



**HAL**  
open science

# Universality class change from Mean-Field to 3D-Heisenberg in magnetocaloric compounds $\text{SmNi}_{3-x}\text{Fe}_x$

H. Jaballah, K. Nouri, N. Mliki, Lotfi Bessais, M. Jemmali

► **To cite this version:**

H. Jaballah, K. Nouri, N. Mliki, Lotfi Bessais, M. Jemmali. Universality class change from Mean-Field to 3D-Heisenberg in magnetocaloric compounds  $\text{SmNi}_{3-x}\text{Fe}_x$ . *Chemical Physics Letters*, 2022, 787, pp.139260. 10.1016/j.cplett.2021.139260 . hal-03983765

**HAL Id: hal-03983765**

**<https://hal.science/hal-03983765>**

Submitted on 8 Jan 2024

**HAL** is a multi-disciplinary open access archive for the deposit and dissemination of scientific research documents, whether they are published or not. The documents may come from teaching and research institutions in France or abroad, or from public or private research centers.

L'archive ouverte pluridisciplinaire **HAL**, est destinée au dépôt et à la diffusion de documents scientifiques de niveau recherche, publiés ou non, émanant des établissements d'enseignement et de recherche français ou étrangers, des laboratoires publics ou privés.



Distributed under a Creative Commons Attribution - NonCommercial 4.0 International License

# Universality class change from Mean-Field to 3D-Heisenberg in magnetocaloric compounds $\text{SmNi}_{3-x}\text{Fe}_x$ .

H. Jaballah,<sup>1,2</sup> K. Nouri,<sup>3</sup> N. Mliki,<sup>2</sup> L. Bessais,<sup>1</sup> and M. Jemmal<sup>4,5</sup>

<sup>1</sup>*Univ Paris Est Creteil, CNRS, ICMPE, UMR 7182, 2 rue Henri Dunant, F-94320 Thiais, France*

<sup>2</sup>*Université de Tunis El Manar, Faculté des Sciences de Tunis,  
Lab Mat Org & Propriétés LR99ES17, Tunis 2092, Tunisia.*

<sup>3</sup>*Capgemini Engineering, Direction Research & Innovation Department,  
2 rue Paul Dautier, 78140, Vélizy-VillaCoublay, France*

<sup>4</sup>*University of Sfax, Faculty of Sciences, LSME, BP1171, Sfax 3018, Tunisia.*

<sup>5</sup>*Department of Chemistry, College of Science and Arts, Ar-rass,  
Qassim University, PO Box 53, Buraydah Postcode 51921, Saudi Arabia.*

(Dated: November 18, 2021)

We report a study of universality class change from Mean-Field to 3D-Heisenberg in magnetocaloric compounds  $\text{SmNi}_{3-x}\text{Fe}_x$ . Three conventional techniques are used to identify the universal classes: the Modified Arrott plot, Kouvel-Fisher plot, and critical isotherm technique. The calculated critical exponents were confirmed and the isotherm  $M(H)$  curves in paramagnetic state and ferromagnetic state fall in two separated universal branches. The exponents found are similar to those determined from the renormalization group approach for a heuristic mean-field ( $d = 3, n = 3$ ) and 3D-Heisenberg ( $d = 3, n = 3$ ) model for  $\text{SmNi}_3$  and  $\text{SmNi}_{2.2}\text{Fe}_{0.8}$ , respectively.

PACS numbers: 75.50.Bb, 75.50.Tt, 76.80.+y

Keywords: Intermetallic rare-earth transition-metal compounds; Phase transitions; Critical exponents.

## I. INTRODUCTION

Intermetallic (R-T) compounds combining rare-earth (R) and transition metal (T) atoms have attracted intense interest due to their extensive applications. R-T compounds were studied in several works for their thermodynamic properties[1], thermal hysteresis [2], hydrogen absorption[3, 4], thermal expansion properties, and magnetocaloric effect (MCE) [5–8]. Rare earth-transition metal is one of the most used materials in technology because of its structural properties, leading to a range of functional magnetic properties [9]. The Curie temperature ( $T_C$ ) in rare earth intermetallics represents a direct measure of the exchange interaction responsible for ferromagnetism. This interaction depends strongly on the interatomic distance, the magnetic moment of the transition metal atom, and the de Gennes factor of the rare-earth atom.

Among the R-T intermetallics, we are interested in  $\text{RT}_3$ . The study of its structures shows that the  $\text{RT}_3$  series crystallizes in two type structures, the hexagonal  $\text{CeNi}_3$  ( $P6_3mm/c$ -space group) and the rhombohedral  $\text{PuNi}_3$  ( $R\bar{3}m$ -space group) depending to the rare earth or metal transition [10, 11]. One of the most known series is  $\text{RNi}_3$  [12–18]. Investigation of thermomagnetic properties shows that the  $T_C$  of  $\text{RNi}_3$  are very low compared to  $\text{RT}_3$  compounds; these results can be explained by the small value of the magnetic moment of Ni atom. Partial substitution of Ni by other atoms with a higher magnetic moment can influence the magnetic properties and increase  $T_C$  value. In previous work by our group, it has been demonstrated the existence and the stability of pure  $\text{SmNi}_{3-x}\text{Fe}_x$  compounds, in the framework of the study of the isothermal section at 1073 K of the

$\text{Sm-Fe-Ni}$  ternary system, it was established in the whole concentration range, using X-ray powder diffraction and energy dispersive X-ray spectroscopy by scanning electron microscopy (SEM/EDS) [19]. XRD patterns of compounds and the purity of the  $\text{SmNi}_{3-x}\text{Fe}_x$  were studied and verified. The ternary system  $\text{SmNi}_{3-x}\text{Fe}_x$  crystallizes in the rhombohedral  $\text{PuNi}_3$  ( $R\bar{3}m$ -space group), can be described by stacking along the  $c$  axis of  $\text{RT}_5$  ( $\text{CaCu}_5$ -type structure) and  $\text{SmNi}_2$  ( $\text{MgCu}_2$ -type structure) unit blocks. The results of Rietveld refinement for  $\text{SmNi}_{3-x}\text{Fe}_x$  show slight increase in the lattice parameters after the substitution of Ni atom by iron one, for  $x=0$   $a$  and  $c$  are equal to  $5.0706(2)\text{\AA}$  and  $5.0710(4)\text{\AA}$ , respectively, however, for  $x=0.8$   $a$  and  $c$  are equal to  $24.7643(1)\text{\AA}$  and  $24.8101(4)\text{\AA}$ , respectively.

Most of  $\text{RNi}_3$  compound exhibits a second-order magnetic phase transition, which often manifests itself by the appearance of a new property of matter, characterized by a macroscopic variable resulting from cooperative or collective phenomena on a microscopic scale. The macroscopic thermodynamic quantities follow a critical behavior in power laws in the vicinity of the transition temperature. The range of validity in temperature of these laws extends over the area of critical fluctuations. The power laws of the critical isotherm (CI) at  $T_C$ , magnetization with zero magnetic field and the inverse of magnetic susceptibility are characterized by three critical exponents (CE) which are:  $\delta$ ,  $\beta$ , and  $\gamma$ , respectively. Previous studies [20–25] on the critical behavior around the order temperature have suggested that CE play a key role in understanding the interaction mechanisms.

In this research, we studied the influence of the substitution of Ni atom with Fe one on the critical behavior near  $T_C$ , the nature as well as the range of interaction,

and the magnetocaloric effect in  $\text{SmNi}_3$  and  $\text{SmNi}_{2.2}\text{Fe}_{0.8}$  samples.

## II. EXPERIMENTS

$\text{SmNi}_3$  and  $\text{SmNi}_{2.2}\text{Fe}_{0.8}$  were prepared from high purity elements samarium 99.98%, nickel 99.9%, and iron 99.9% by arc-melting technique under a purified argon atmosphere. The elements were placed in a copper crucible cooled by cold water. After ingot formation, the compound was wrapped into tantalum foil and introduced into a silica tube sealed under secondary vacuum  $2 \times 10^{-6}$  bar [26, 27]. The ingot was heat-treated for seven days at 1073 K and finally, water quenched [28, 29]. A Physical Properties Measurement System (PPMS) magnetometer was used for measurements at low temperatures. Isotherms were collected at an interval of 1 K around  $T_C$  with an applied magnetic field up to 5 T. To get the internal field  $H_{\text{int}}$ , the external applied magnetic field  $H_{\text{ext}}$  was corrected for the demagnetization effect using  $H_{\text{int}} = H_{\text{ext}} - N_d M(T, H_{\text{ext}})$ . Demagnetization constant  $N_d$  was determined from  $M$  vs  $H_{\text{ext}}$  curve in low field region following the method given in Ref [30].

## III. SCALING ANALYSIS

According to Ref.[31] in the vicinity of  $T_C$  the correlation length, spontaneous magnetization, the inverse of magnetic susceptibility, and  $M(H)$  at  $T = T_C$  follow a power law, each one is defined by a CE.

Near  $T_C$  in a second-order phase transition, the correlation length is defined as follow:

$$\xi(T) = \xi_0 |(T - T_C)/T_C|^{-\nu} \quad (1)$$

For the spontaneous magnetization  $M_s$  below  $T_C$ , the inverse initial susceptibility  $\chi_0^{-1}$  above  $T_C$  and the measured magnetization  $M(H)$  at  $T_C$  are characterized by the following scaling laws:

$$M_s(T) = M_s(0)(-\epsilon)^\beta, \epsilon < 0, T < T_C \quad (2)$$

$$\chi_0^{-1}(T) = \chi_0^{-1}(0)(\epsilon)^\gamma, \epsilon > 0, T > T_C \quad (3)$$

$$M = DH^{1/\delta}, \epsilon = 0, T = T_C \quad (4)$$

where  $M_s(0)$ ,  $\chi_0^{-1}(0)$ , and  $D$  are the critical amplitudes and  $\epsilon = (T - T_C)/T_C$  is the reduced temperature [31]. According to the scaling hypothesis in the asymptotic critical region, the magnetic equation, which is a relationship between the variables  $T$ ,  $\mu_0 H$ , and  $(H, \epsilon)$ , can be expressed as follows:

$$M(H, \epsilon) = \epsilon^\beta f_\pm(H/\epsilon^{\beta+\gamma}) \quad (5)$$

where  $f_-$  for  $T < T_C$  and  $f_+$  for  $T > T_C$  are the regular functions. By writing magnetization and magnetic field in these renormalized forms, renormalized magnetization  $m \equiv \epsilon^{-\beta} M(H, T)$  and renormalized field  $h \equiv \epsilon^{-\beta+\gamma} H$ , Eq. (5) can be written as:

$$m = f_\pm(h) \quad (6)$$

This means that for proper scale relationships and the appropriate selection of  $\beta$ ,  $\gamma$ , and  $\delta$  values, scaled  $m$ , and  $h$  will fall on two universal curves above and below  $T_C$ . Scaled  $m$  and  $h$  is an essential criterion to check the validity of the selected CE.

## IV. RESULTS AND DISCUSSIONS

### A. Magnetic properties

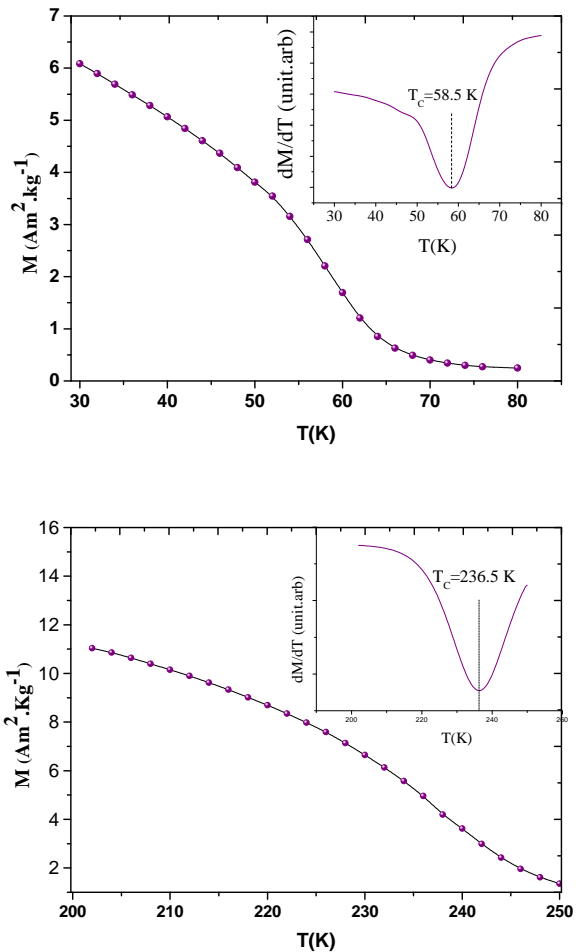


Figure 1. Temperature dependence of magnetization measured at  $\mu_0 H = 0.1$  T with  $dM/dT$  for  $\text{SmNi}_3$  and  $\text{SmNi}_{2.2}\text{Fe}_{0.8}$ .

The temperature dependence of magnetization for  $\text{SmNi}_3$  and  $\text{SmNi}_{2.2}\text{Fe}_{0.8}$  compounds measured under an external applied magnetic field of 0.1 T is shown in Fig. 1. We calculate  $T_C$  value defined as the minimum of  $dM/dT$  curve. For  $\text{SmNi}_3$ ,  $T_C$  is equal to 58.5 K. After substituting nickel by iron atom,  $T_C$  increases significantly from 58.5 K to 236.5 K.

$T_C$  in rare-earth intermetallics represents a direct measure of the exchange interaction, which is responsible for ferromagnetism. This interaction depends strongly on the magnetic moment of the transition metal atom. The magnetic moment of the iron atom is higher than the magnetic moment of the nickel atom, this can explain the significant increase of  $T_C$  value. This result is in good agreement with previous works in literature, indeed, A. Bajorek *et al.* [32] found that in  $\text{GdNi}_{3-x}\text{Fe}_x$  the  $T_C$  increases with iron content.

Based on Banerjee's criteria [33], the order of transition is second or first order depending on slope sign negative or positive. A negative slope corresponds to the first-order transition while positive corresponds to the second-order. The shape of the curves in Fig. 7 and Fig. 9 shows a positive slope which indicates that  $\text{SmNi}_3$  and  $\text{SmNi}_{2.2}\text{Fe}_{0.8}$  exhibit a second-order one.

## B. Critical study

### 1. Modified Arrott plot method

In most cases, to identify the CE and critical temperature, Arrott method is used [34]. This method supposes that the CE follow the mean-field (M-F) theory, with  $\beta = 0.5$  and  $\gamma = 1.0$  [34]. Based on this assumption, the isotherms  $M^2$  vs  $H/M$  constitute a set of parallel straight lines, and the isotherm that correspond to  $T_C$  is a straight line that passes through the origin. Fig. 4 show that the isotherms around  $T_C$  of  $\text{SmNi}_3$  compounds exhibit a linear behavior with the same slope. The critical exponent of the M-F model is the most appropriate for this compound. Contrary to the Arrott plot, all curves in Fig. 4, Fig. 5 and Fig. 6 shows a non-linear behavior even in the high region field, this indicates that the 3D-Ising (3D-I), 3D-Heisenberg model (3D-H), and tricritical M-F model are not appropriate for our compound.

Fig. 7 shows that all isotherms of  $\text{SmNi}_{2.2}\text{Fe}_{0.8}$  exhibit a nonlinear behavior having a downward curvature also for high  $\mu_0 H$  values. It implies that the critical exponent of the M-F model is not appropriate for our compound. To clarify the nature of magnetic transition phase we have used the modified Arrott plot (MAP) of  $M^{1/\beta}$  vs  $(H/M)^{1/\gamma}$  [35]. The Arrott-Noakes equation of state that gives the MAP is defined as:

$$(H/M)^{1/\gamma} = a\epsilon + bM^{1/\beta} \quad (7)$$

where  $\epsilon = (T - T_C)/T_C$  is the reduced temperature, and  $a$  and  $b$  are constants. To construct the MAP four model

are used: 3D-H model ( $\beta = 0.365, \gamma = 1.386$ ), 3D-I ( $\beta = 0.325, \gamma = 1.241$ ), 3D-XY model ( $\beta = 0.325, \gamma = 1.241$ ) and tricritical M-F model ( $\beta = 0.25, \gamma = 1.0$ ) [36], as shown in Fig. 8-10. As we can see, three MAP using 3D-I, 3D-H and 3D-XY exhibit quasi straight lines in the high-field region. It is easy to see that the isotherms in Fig. 11 exhibits a curved line, showing that the tricritical M-F model is not the appropriate model for our compound. Nevertheless, all the lines in Fig. 8, Fig. 9 and Fig. 10 are approximately paralleling each other. To find the most suitable model, we can use the normalized slope ( $NS$ ) is defined as  $NS = S(T)/S(T_c)$  where  $S(T)$  is the slope of isotherm at temperature  $T$  in high field region [37], For the most adequate model, the MAP should be a series of parallel lines in the high-field region with the same slope, consequently  $NS = S(T)/S(T_c) \sim 1$ . Fig. 2 shows that for  $\text{SmNi}_{2.2}\text{Fe}_{0.8}$  sample M-F and tricritical M-F models clearly deviate from  $NS = S(T)/S(T_c) = 1$ , the same observation for 3D-I model and 3D-XY model but in a less significant way. Furthermore,  $NS = S(T)/S(T_c)$  of 3D-H model is close to 1 with slight deviation. To

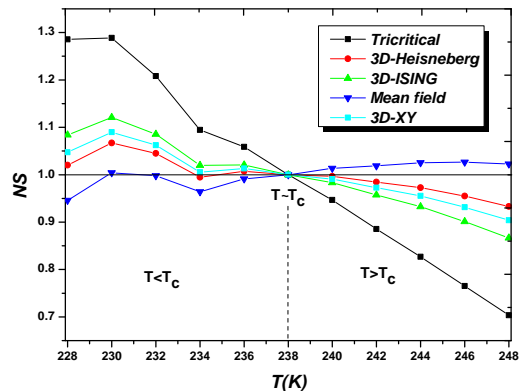
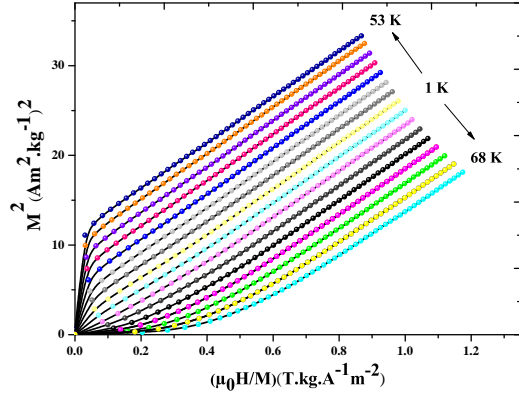
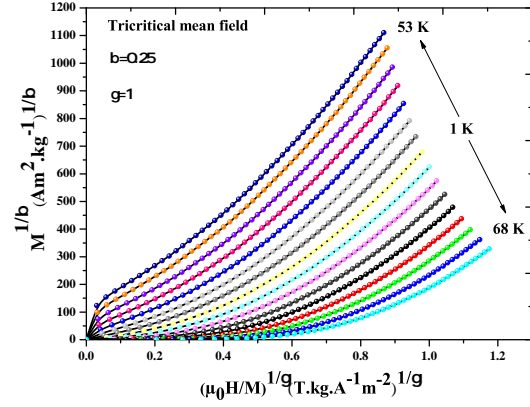
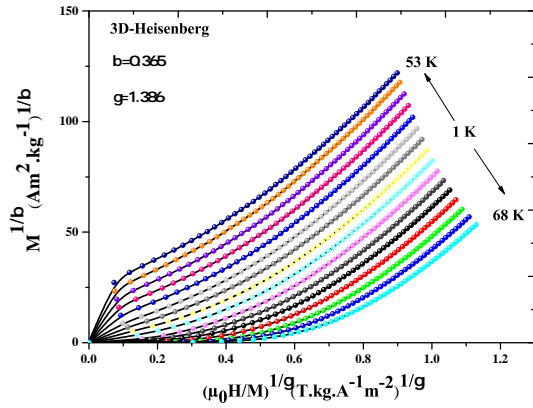
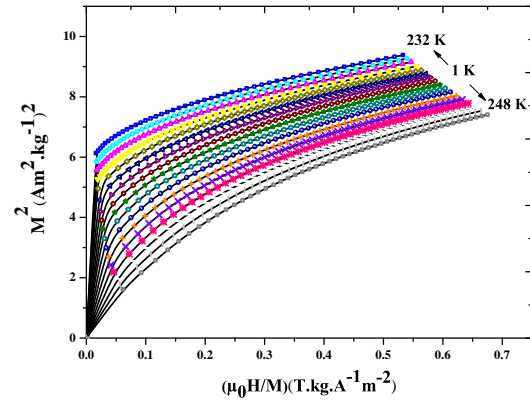
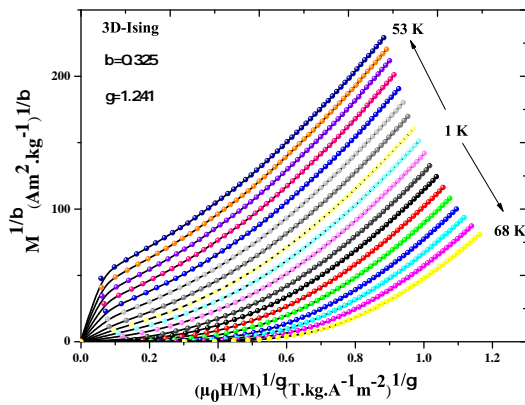
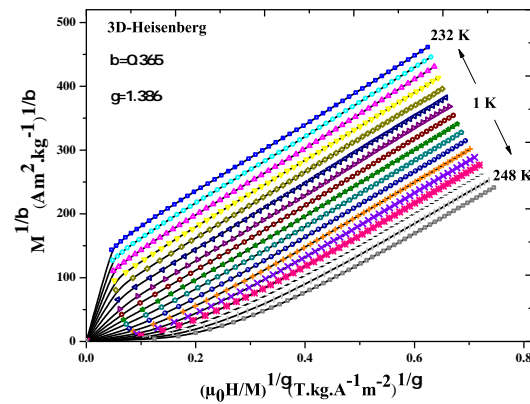


Figure 2. Temperature dependence of the normalized slopes Normalized slope for  $\text{SmNi}_{2.2}\text{Fe}_{0.8}$ .

calculate with more precision the appropriate CE  $\gamma$  and  $\beta$  for our compounds, a rigorous iterative method was used [38]. A linear extrapolation from the high-field region which gives the spontaneous magnetization ( $M_s(T)$ ) and the inverse of initial magnetic susceptibility  $\chi_0^{-1}(T)$  as an intercept of  $M^{1/\beta}$  and  $(H/M)^{1/\gamma}$  axis, respectively.

The obtained data by the linear extrapolation is fitted using the Eq. (2) and Eq. (3). A new MAP is then reconstructed using the new values of  $\beta$  and  $\gamma$ . As a result, new data from linear extrapolation is obtained. So, new values of  $\beta$  and  $\gamma$  can be obtained. This exercise was repeated until the values of  $\beta$ , and  $\gamma$  are stable. Fig. 12 show the final  $M_s(T)$  and  $\chi_0^{-1}(T)$  with fitting curves and values of  $\beta$  and  $\gamma$  and  $T_C$  are obtained.

Figure 3. Arrott plot for  $\text{SmNi}_3$ .Figure 6. MAP using tricritical M-F model exponents  $\text{SmNi}_3$ .Figure 4. MAP using 3D-H model exponents for  $\text{SmNi}_3$ Figure 7. Arrott plot for  $\text{SmNi}_{2.2}\text{Fe}_{0.8}$ .Figure 5. MAP using 3D-I model exponents for  $\text{SmNi}_3$ Figure 8. MAP using 3D-H model exponents for  $\text{SmNi}_{2.2}\text{Fe}_{0.8}$ .

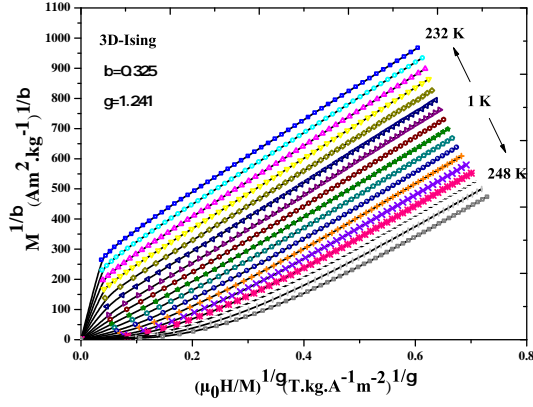


Figure 9. MAP using 3D-I model exponents for  $\text{SmNi}_{2.2}\text{Fe}_{0.8}$ .

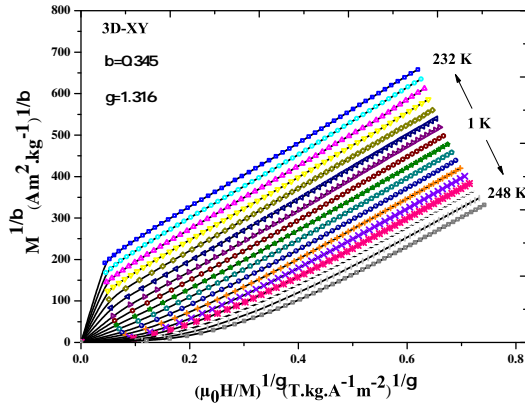


Figure 10. MAP using 3D-XY model exponents for  $\text{SmNi}_{2.2}\text{Fe}_{0.8}$ .

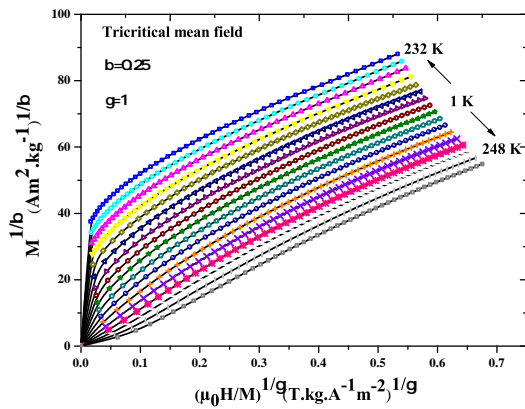


Figure 11. MAP using tricritical M-F model exponents for  $\text{SmNi}_{2.2}\text{Fe}_{0.8}$ .

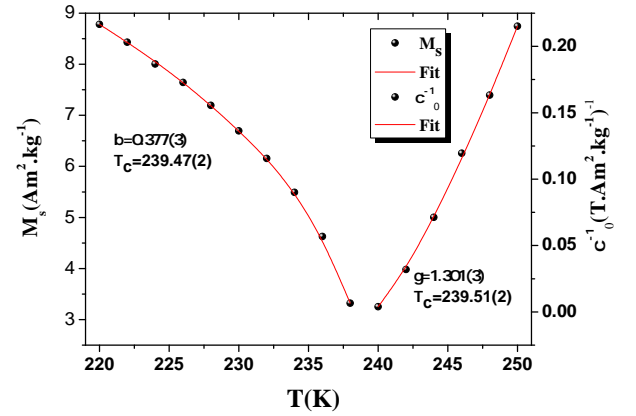
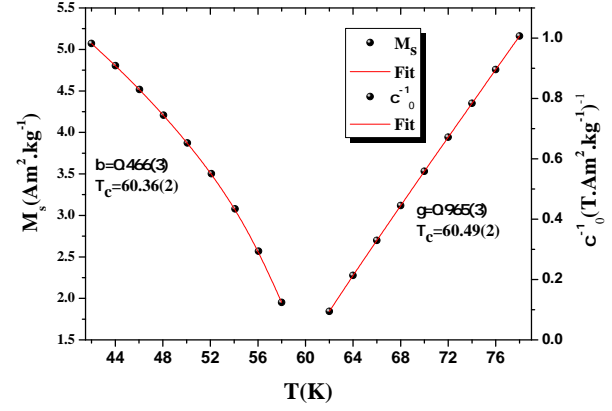


Figure 12. Temperature dependence of the spontaneous magnetization  $M_s(T)$  (left) and the inverse initial susceptibility  $\chi_0^{-1}(T)$  (right) with solid fitting curves for  $\text{SmNi}_3$  and  $\text{SmNi}_{2.2}\text{Fe}_{0.8}$ .

## 2. Kouvel Fisher method

To determine the CE more accurately Kouvel-Fisher (KF) method should be employed [39]:

$$M_s(T)/(dM_s(T)/dT) = (T - T_C)/\beta$$

$$\chi_0^{-1}(T)/(d\chi_0^{-1}(T)/dT) = (T - T_C)/\gamma$$

Following this method,  $\chi_0^{-1}(T)/(d\chi_0^{-1}(T)/dT)$  and  $M_s(T)/(dM_s(T)/dT)$  are a linear functions of temperature with slopes of  $1/\gamma$  and  $1/\beta$  and intercepts temperature axis for  $T = T_C$ , respectively. Fig. 13 show the linear fits that gives  $\beta$  with  $T_C$  and  $\gamma$  with  $T_C$ .

## 3. Isotherm method

Fig. 14 show the isothermal magnetization  $M(H)$  at a critical temperature  $T_C$ , inset is the same plot on a log-log scale. Based on Eq. (4) the value of  $\delta$  can be

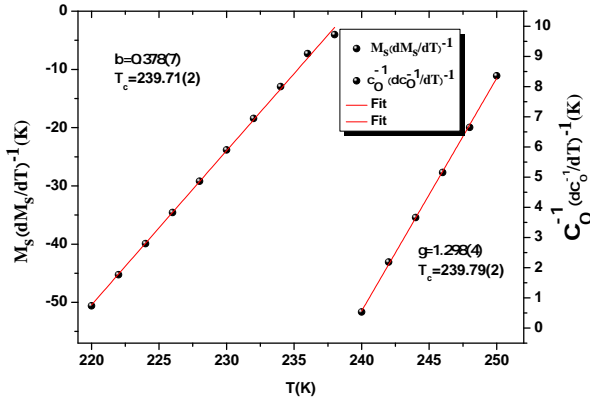
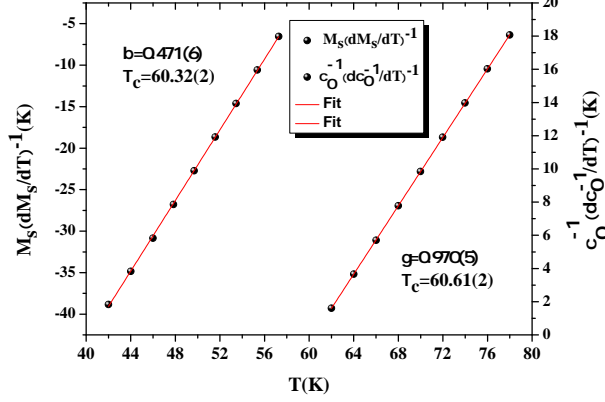


Figure 13. (b) KF plots of  $M_s(T)/(dM_s(T)/dT)$  (left) and  $\chi_0^{-1}(T)/(d\chi_0^{-1}(T)/dT)$  (right) with solid fitting curves for  $\text{SmNi}_3$  and  $\text{SmNi}_{2.2}\text{Fe}_{0.8}$ .

easily determined with a linear fit  $\log(M)$  at  $T = T_C$ . Widom scaling law can be used to calculate the third exponent  $\delta$  as follow,  $\delta = 1 + \gamma/\beta$ . Using the  $\beta$  and  $\gamma$  values determined from the MAP and KF plot, we obtain  $\delta$  values (Tab I). The obtained value of  $\delta$  by fitting the CI is very close to the values obtained from the MAP and KF plots. The CE for  $\text{SmNi}_3$  and  $\text{SmNi}_{2.2}\text{Fe}_{0.8}$  samples are similar to those of the M-F model and 3D-H, respectively. They are suggesting that the partial substitution of Ni by Fe atom has an influence on the critical regime and in contrast to  $T_C$  value.

#### 4. Effective CE

Because of the deviation of the deduced exponents in the present study from the conventional theoretical values, it is important to clarify if  $\text{SmNi}_3$  and  $\text{SmNi}_{2.2}\text{Fe}_{0.8}$  compounds belong to the founded universality class (in this study) as they approach the asymptotic limit. For this purpose, we introduce effective CE  $\beta_{\text{eff}}$  and  $\gamma_{\text{eff}}$ , they are calculated using Eq. (8) and Eq. (9) [39].

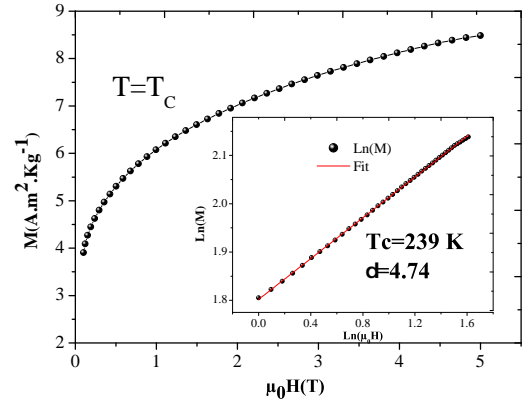
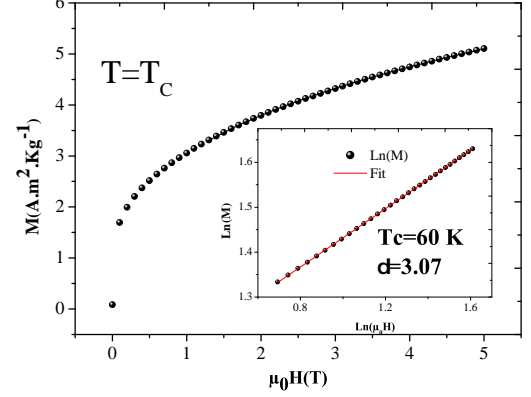


Figure 14. Isothermal magnetic curves at  $T_C$  for  $\text{SmNi}_3$  and  $\text{SmNi}_{2.2}\text{Fe}_{0.8}$  samples. The insets show these plots in logarithmic scale

$$\beta_{\text{eff}}(\epsilon) = \frac{d \ln(M_s(\epsilon))}{d \ln(\epsilon)} \quad (8)$$

$$\gamma_{\text{eff}}(\epsilon) = \frac{d \ln(\chi_0^{-1}(\epsilon))}{d \ln(\epsilon)} \quad (9)$$

It is seen that both  $\beta_{\text{eff}}$  and  $\gamma_{\text{eff}}$  show monotonic change with  $\epsilon$  even in the asymptotic critical region for  $\text{SmNi}_3$  indicating that the exponents obtained are not those which appear around an intersection region between two universality classes. A non monotonic change of effective exponents with  $\epsilon$  can be explained by: (I) System goes through crossover regime to another universality class in asymptotic regime [40], (II)  $\epsilon_{\text{min}}$  is not falling in the asymptotic regime, and  $T_C$  must be approximated more closely to have asymptotic exponents, and (III)  $\epsilon_{\text{min}}$  is in the asymptotic region, in fact, it was observed in disordered materials in the asymptotic regime that effective exponents does not match with the universality classes [41]. For  $\text{SmNi}_3$ , the monotonic changes of  $\beta_{\text{eff}}$  and  $\gamma_{\text{eff}}$  with reduced temperature are attributed to magnetic orders. On the other hand, for  $\text{SmNi}_{2.2}\text{Fe}_{0.8}$  (b) we can

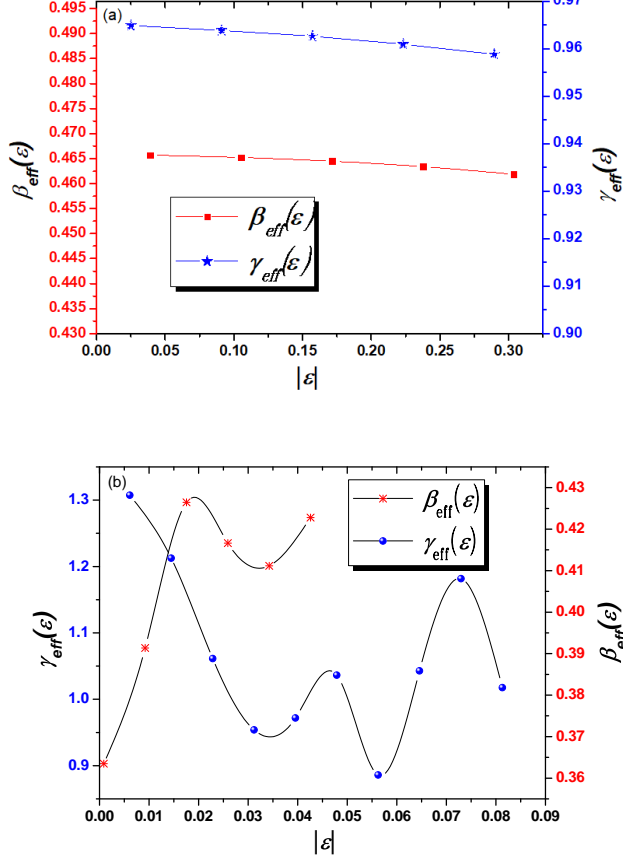


Figure 15. Effective exponents are plotted as a function of reduced temperature  $\epsilon$  for  $SmNi_{13}$ (a) and  $SmNi_{2.2}Fe_{0.8}$ (b) samples.

see that,  $\beta_{eff}$  show nonmonotonic change with  $\epsilon$  in the asymptotic critical region, and  $\gamma_{eff}$  decrease rapidly with  $\epsilon$  before returning to a M-F value and goes through the peak at higher  $\epsilon$ , which is considered as characteristic features of a disordered ferromagnet below  $T_C$  [41]. Indeed, the  $RT_3$  compounds are obtained by the stacking of  $R_2T_4$  and  $RT_5$  unit block three times. The unit cell contains two nonequivalent crystallographic sites for  $R$  ions  $3a(0,0,0)$  and  $6c(0,0,z)$ , and three sites for  $T$ :  $3b(0,0,0.5)$ ,  $6c(0,0,z)$  and  $18h(0.5,0.5,z)$ . This disorder can be explained by the in-homogeneous distribution of iron atom and nickel atom on the three crystallographic sites of the transition metal, which are not similar in terms of magnetic moment value. Similar nonmonotonic change of  $\gamma_{eff}$  and  $\beta_{eff}$  was observed in antiperovskite material  $AlCMn_3$  [42], this behavior was attributed to magnetic disorder due to few disorder in atomic distribution in  $AlCMn_3$  sample, also a similar behavior was observed in cubic praseodymium oxides perovskites  $Pr_{0.5}Sr_{0.5}MnO_3$ , the nonmonotonic change was attributed to magnetic disorder arises from dissimilar ions ( $P_1^{3+}$ ,  $Sr^{2+}$ ) and/or inhomogeneous phases below and above  $T_C$

[38]. In the critical region when  $T \sim T_C$  ( $\epsilon \rightarrow 0$ ), effective exponents  $\beta_{eff}(\epsilon)$  and  $\gamma_{eff}(\epsilon)$  should  $\sim$  to real exponents value  $\beta$  and  $\gamma$ . Around  $T_C$  ( $\epsilon \rightarrow 0$ ), we found ( $\beta_{eff}=0.465$ ,  $\gamma_{eff}=0.964$ ) for  $SmNi_{13}$ , which approach to CE observed experimentally ( see Tab I), and ( $\beta_{eff}=0.428$ ,  $\gamma_{eff}=0.903$ ) for  $SmNi_{2.2}Fe_{0.8}$  which does not much with any universal classes, even we tried to plot MAP using  $\beta_{eff}=0.428$  and  $\gamma_{eff}=0.903$ , and all curves show a non linear behavior even in the high field region.

### 5. Validity of CE

The validity and reliability of  $\beta$ ,  $\gamma$ ,  $\delta$  and,  $T_C$  can also be checked following Eq. (5) and Eq. (6), scaled M vs scaled  $\mu_0 H$  and renormalized scaled  $M \equiv m$  vs renormalized scaled  $H \equiv h$  was plotted in Fig. 16 and Fig. 17, respectively, insets of Fig. 16 show the same plots on a log-log scale. It is fairly easy to see that all the data collapse into two separate branches: one below  $T_C$  and another above  $T_C$ . This result validates the values of  $\beta$ ,  $\gamma$ ,  $\delta$ .

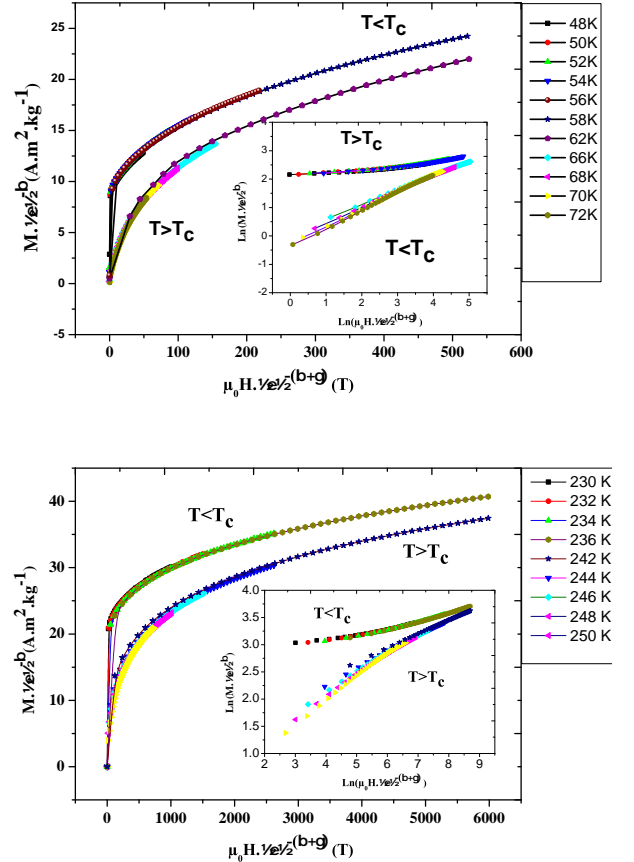


Figure 16. Scaling plots indicating two universal curves below and above  $T_C$  for  $SmNi_{13}$  and  $SmNi_{2.2}Fe_{0.8}$  samples. Inset show the same plots on a log-log scale.

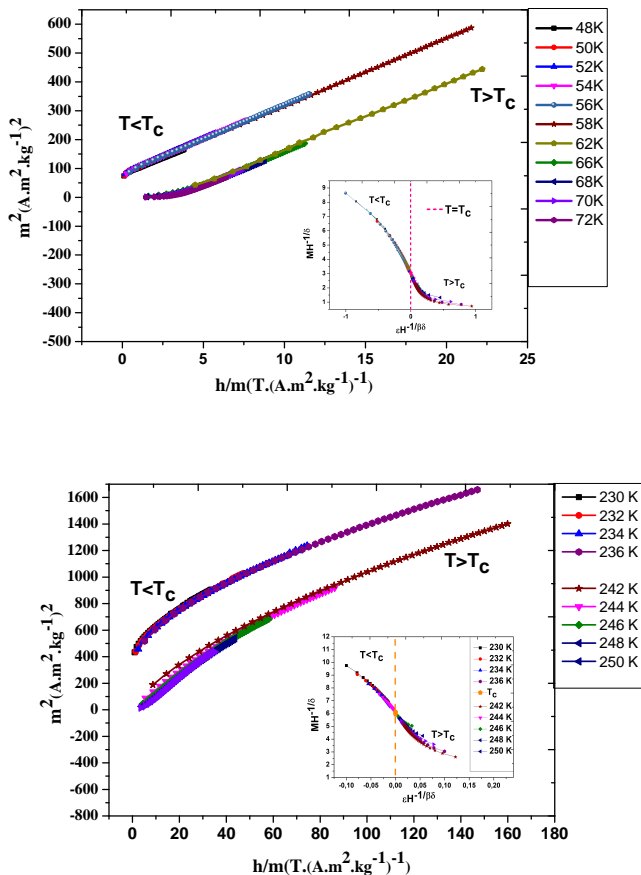


Figure 17. The renormalized magnetization and field replotted in the form of  $m^2$  vs  $h/m$  for  $\text{SmNi}_3$  and  $\text{SmNi}_{2.2}\text{Fe}_{0.8}$  samples. (Inset) The rescaling of the  $M(H)$  curves by  $MH^{-1/\delta}$  vs  $\epsilon^{1/\gamma+\beta}$

Table I. Values of the exponents  $\beta$ ,  $\gamma$  and  $\delta$  as determined from the MAP, KF plot, and the CI techniques are given for  $\text{SmNi}_3$  (a) and  $\text{SmNi}_{2.2}\text{Fe}_{0.8}$  (b). The theoretically predicted values of exponents for various universality classes M-F, 3D-H and 3D-I are given for the sake of comparison.

<sup>w</sup> Calculated from Widom scaling relation $\delta = 1 + \gamma/\beta$					
	Ref.	Technique	$\beta$	$\gamma$	$\delta$
a	This Work	MAP	0.466(3)	0.965(3)	3.07(3) <sup>w</sup>
	-	KF	0.471(6)	0.971(5)	3.06(5) <sup>w</sup>
	-	CI	-	-	3.08(2)
b	This Work	MAP	0.377(3)	1.301(3)	4.45(4) <sup>w</sup>
	-	KF	0.378(7)	1.298(4)	4.43 (8) <sup>w</sup>
	-	CI	-	-	4.74 (2)
M-F	[36]	Theory	0.5	1	3
3D-H	[36]	Theory	0.365	1.386	4.79
3D-I	[36]	Theory	0.325	1.241	4.82
3D-XY	[36]	Theory	0.345	1.316	4.81

In addition, it is important to check if all CE:  $\beta$ ,  $\gamma$ , and  $\delta$  can generate the scaling equation of state using another form of the equation of states:

$$MH^{1/\delta} = S(\epsilon/H^{1/\beta\delta}) \quad (10)$$

where  $S(t)$  is the scaling function. According to Eq. (10), all isotherms will collapse into a unique curve. The inset Fig. 17 shows that the CE  $\beta$ ,  $\gamma$ , and  $\delta$  have successfully generate the scaling equation for both compounds  $\text{SmNi}_3$  and  $\text{SmNi}_{2.2}\text{Fe}_{0.8}$ . Where the experimental data collapse into a unique curve. This result confirm the validity and the reliability of the obtained CE. Tab I show the obtained CE of  $\text{SmNi}_3$  and  $\text{SmNi}_{2.2}\text{Fe}_{0.8}$  determined by various techniques exhibit a slight deviation from the M-F model and 3D-H model.

### 6. Spin interaction range

One can see that the CE of  $\text{SmNi}_3$  are close to those predicted by the M-F theory. Furthermore, the obtained CE for  $\text{SmNi}_{2.2}\text{Fe}_{0.8}$  is in between 3D-H model and 3D-XY model, in fact,  $\gamma$  approaches to  $\gamma$  of the 3D XY and  $\beta$  approaches to the value predicted by 3D-H. Then it is crucial to understand the nature as well as the range of interaction in this compounds. According to renormalization group theory, the spin interaction degrades with distance  $r$  as  $J(r) = r^{-3+\sigma}$ , where  $\sigma$  is a positive constant [43]. In addition, the susceptibility exponent  $\gamma$  depend on  $\sigma$ ,  $d$  and  $n$ ,  $\gamma$  is predicted as:

$$\gamma = 1 + \left(\frac{4}{d}\right)\left(\frac{n+2}{n+8}\right)\Delta\sigma + \frac{8(n+2)(n-4)}{d^2(n+8)^2} \times \left[1 + \frac{(G(\frac{d}{2})(7n+20))}{(n-4)(n+8)}\right]\Delta\sigma^2 \quad (11)$$

Where  $\Delta\sigma = (\sigma - d/2)$ ,  $d$  and  $n$  is dimensionality of the system and the spin, respectively. According to this model, if  $\sigma < 2$  indicates that the range of spin interaction is long, but, if  $\sigma > 2$  the range of spin interaction is short. In fact, when  $\sigma > 2$  the 3D-H model is valid,  $J(r)$  decays faster than  $r^{-5}$  with short range type interaction, considering that  $\sigma < 2$  it agrees with M-F model and  $J(r)$  decays slower than  $r^{-4.5}$ . In the range between short range and long range ( $1.5 < \sigma < 2$ )  $J(r)$  decays slower than  $r^{-5}$  and faster than  $r^{-4.5}$ , the CE take intermediate values between tow classes. In our case, for  $\text{SmNi}_3$  it is found from Eq. 11 that  $[d : n] \equiv [3 : 3]$  and  $\sigma = 1.448$  give the exponents ( $\beta = 0.519$ ,  $\gamma = 0.97$ , and  $\delta = 2.87$ ), which are mostly close to our experimentally observed values Tab. I. In recent study of critical behavior for the inter-metallic compound  $\text{Y}_2\text{Fe}_{17}$  [44], the authors have found that the spin interaction range decays as  $J \sim r^{-3.4274}$  with space dimensionality  $d=2$ , spin dimensionality  $n=2$  and  $\sigma = 1.4274$ , the value of  $\sigma$  is less than 2 which is the signature of long interaction. This result is in agreement

with the value of  $\sigma$  for  $\text{SmNi}_3$  sample. For  $\text{SmNi}_{2.2}\text{Fe}_{0.8}$ , we obtain ( $\beta = 0.386$ ,  $\gamma = 1.354$ , and  $\delta = 4.51$ ) for  $n=d=3$  and  $\sigma = 1.91$  which are close to our experimentally observed. In addition, we can calculate the  $\xi$  critical exponent  $\nu = 0.708$  [ $\nu = \gamma/\sigma$ ] [ $\xi = |\xi_0|(T - T_C)/T_C|^{-\nu}$ ], and  $\alpha = -0.126$  ( $\alpha = 2 - \nu.d$ ),  $\alpha$  value of  $\text{SmNi}_{2.2}\text{Fe}_{0.8} \sim \alpha(3\text{D-H model})$  [45, 46]. This calculation suggests that the spin interaction  $\text{SmNi}_{2.2}\text{Fe}_{0.8}$  is close to the 3D-H [ $d : n \equiv [3 : 3]$ ] type coupled, the values of  $\sigma$  are close to 2 by lower value, suggesting the ferromagnetic interaction in this compound is at the boundary between a long-range type and a short-range type interaction.

## V. CONCLUSION

In conclusion, we have studied in details the critical behavior around  $T_C$  in  $\text{SmNi}_3$  and  $\text{SmNi}_{2.2}\text{Fe}_{0.8}$ . Both of  $\text{SmNi}_3$  and  $\text{SmNi}_{2.2}\text{Fe}_{0.8}$  exhibit a second transition.  $\beta$ ,  $\gamma$ , and  $\delta$  were obtained using conventional methods, the reliability and the validity of the founded  $\beta$ ,  $\gamma$ , and

$\delta$  were confirmed. For  $\text{SmNi}_3$ , the determined exponents are close to M-F model( $d = 3 : n = 3$ ) spins coupled with a long-range interaction type ( $\sigma = 1.448$ ), spin decays as  $J(r) = r^{-(4.448)}$  with  $\sigma = 1.448$ . For  $\text{SmNi}_{2.2}\text{Fe}_{0.8}$ , the determined exponents are close to 3D-H ( $d = 3 : n = 3$ ) spins coupled with an interaction at the boundary between a long-range type and a short-range type ( $\sigma = 1.95$ ) interaction. Spin decays as  $J(r) = r^{-4.95}$ .

## VI. ACKNOWLEDGMENTS

This work was supported by the University of Sfax, Faculty of Science, LSME, by the National Center for Scientific Research (CNRS), France, by the “Ministère de l’Enseignement Supérieur et de la Recherche Scientifique”(LMOP LR99ES17) Laboratory, Tunisia. The authors would like to acknowledge PRF2019-D4P2, PHC-Utique 21G1408, and Tuniso-Marrocaïn 20/R&D23 projects for financial support.

- 
- [1] S. Menouer, OM. Abid, A. Benzair, A. Yakoubi, H. Khachai, and U. Schwingenschlögl. *Sci. Rep.*, 11(1):1–11, 2021.
- [2] RC. Das, A. Pathak, P. Bhorania, and M. Khan. *Bull.Aca.Sci.USSR.Phys*, 2021.
- [3] AN. Kazakov, DV. Blinov, V Yu Bodikov, SV. Mitrokhin, and AA. Volodin. *Int. J. Hydrog*, 46(25):13622–13631, 2021.
- [4] D. Zhang, SJ. Ji, and NT. Suen. *ChemComm*, 57(68):8504–8507, 2021.
- [5] L. Li and M. Yan. *J. Alloys Compd*, 823:153810, 2020.
- [6] Y. Zhang. *J. Alloys Compd*, 787:1173–1186, 2019.
- [7] Y. Wang G. Yaming, D. Guo, B. Wu, S.Geng, and Y. Zhang. *J. Magn. Magn. Mater.*, 498:166179, 2020.
- [8] Y. Zhang, B. Wu, D. Guo, J. Wang, and Z. Ren. *Chin. Phys. B*, 30(1):017501, 2021.
- [9] J-C. Crivello K. Younsi, L. Bessais and V.Russier. *J. Magn. Magn. Mater.*, 340:10–15, 2013.
- [10] Yu. N. Grin L. O. Asylechko and A. A. Fedorchuk. *J. Alloys Compd.*, 219(1-2):222–224, 1995.
- [11] Y. Q. Chen, J. K. Liang, J. Luo, J. B. Li, and G. H. Rao. *Powder Diffract*, 25(4):349–354, 2010.
- [12] K.H.J. Buschow. *Rep. Prog. Phys.*, 40(10):1179, 1977.
- [13] J. Yakinthos and D. Paccard. *Solid State Commun*, 10(11):989–993, 1972.
- [14] D. Paccard and R. Pauthenet. *C. R. Acad. Sci*, 264(15):1056, 1967.
- [15] E. Burzo and F. Givord. *Sci.(France) B*, 271:1158, 1970.
- [16] S.K. Arif and D.S.P. Bunbury. *Phys. Status Solidi A*, 33(1):91–96, 1976.
- [17] S.C. Tsai, C.J. Kunes K.S.V.L Narasimhan, and R.A. Butera. *J. Appl. Phys.*, 45(8):3582–3586, 1974.
- [18] K.S.V.L. Narasimhan, R.A. Butera, and R.S. Craig. *J. Appl. Phys.*, 44(2):879–882, 1973.
- [19] K. Nouri, M. Jemali, S. Walha, K. Zehani, L. Bessais, and A. Ben. Salah. *J. Alloys Compd.*, 661:508–515, 2016.
- [20] AK. Pramanik and A. Banerjee. *Phys.Rev B*, 79(21):214426, 2009.
- [21] Yu. Liu, NV. Ivanovski, and C. Petrovic. *Phys.Rev B*, 96(14):144429, 2017.
- [22] W. Liu, Y. Dai, Y-E. Yang, J. Fan, L. Pi, L. Zhang, and Y. Zhang. *Phys. Rev.B*, 98(21):214420, 2018.
- [23] L. Chen, J. Fan, W. Tong, D. Hu, L. Zhang, L. Ling, L. Pi, Y. Zhang, and H. Yang. *J. Mater. Sci*, 53(1):323–332, 2018.
- [24] L. Xu, J. Fan, W. Sun, Y. Zhu, D. Hu, J. Liu, Y. Ji, D. Shi, and H. Yang. *Appl. Phys. Lett*, 111(5):052406, 2017.
- [25] J. Fan, W. Zhang, X. Zhang, L. Zhang, and Y. Zhang. *Mater. Chem. Phys.*, 144(1-2):206–211, 2014.
- [26] L. Bessais, E. Dorolti, and C. Djega-Mariadassou. *Appl. Phys. Lett.*, 87, 2005.
- [27] S. Khazzan, N. Mliki, L. Bessais, and C. Djega-Mariadassou. *J. Magn. Magn. Mater.*, 322(2):224–229, 2010.
- [28] R. Bensalem, W. Tebib, S. Alleg, J. J. Sunol, L. Bessais, and J. M. Greneche. *J. Alloys Compd.*, 471:24–27, 2009.
- [29] A. Hamrita, Y. Slimani, M. K. Ben Salem, E. Hannachi, L. Bessais, F. Ben Azzouz, and M. Ben Salem. *Ceram. int.*, 40:1461–1470, 2014.
- [30] A. K. Pramanik and A. Banerjee. *J. Phys: Condens. Matter*, 20(27):275207, 2008.
- [31] Michael E Fisher. *Rep. Prog. Phys.*, 30(2):615, 1967.
- [32] A. Bajorek, A. Chrobak, G. Chekowska, and M. Kwiecien. *J.Alloys Compd. 485*, 6, 2009.
- [33] BK Banerjee. *Physics letters*, 12(1):16–17, 1964.
- [34] Anthony Arrott. *Phys Rev*, 108(6):1394, 1957.
- [35] Noakes A. Arrott and E.John. *Phys. Rev. Lett.*, 19(14):786, 1967.
- [36] S. N. Kaul. *J. Magn. Magn. Mater.*, 53(1-2):5–53, 1985.
- [37] J. Fan, L. Ling, B. Hong, L. Zhang, L. Pi, and Y. Zhang. *Phys. Rev. B*, 81(14):144426, 2010.

- [38] AK Pramanik and A Banerjee. *Physical Review B*, 79(21):214426, 2009.
- [39] M. E. Michael J.S. Kouvel. *Phys. Rev.*, 136(6A):A1626, 1964.
- [40] M Haug, M Fähnle, H Kronmüller, and F Haberey. *Journal of Magnetism and Magnetic Materials*, 69(2):163–170, 1987.
- [41] M. Dudka, R. Folk, Yu. Holovatch, and D. Ivaneiko. *J. Magn.Magn. Mate*, 256, 243, 2003.
- [42] L. Zhang, B. Wang, Y. Sun, P.Tong, J. Fan, C. Zhang, L. Pi, and Y. Zhang. *Phys.Rev.B*, 85(10):104419, 2012.
- [43] S-K. Ma ME.Fisher and B. G. Nickel. *Phys Rev Lett*, 29(14):917, 1972.
- [44] J. Fan, C. Huang, H. Liu, Y-E. Yang, JLS. Llamazares, CFS. Valdés, P. Gorria, C. Ma, Y. Zhu, and H. Yang. *CrystEngComm*, 23(18):3411–3418, 2021.
- [45] J. C. LeGuillou and J. Zinn-Justin. *Phys. Rev. B* 21, 3976, (1980).
- [46] M. E. Fisher. *Rev. Mod. Phys.* 46, 597, (1974).